A filtering approach for analyzing turbulent stratified shear flows

Robert E. Ecke[1] and Philippe Odier[2]

[1]Condensed Matter and Magnetic Science and CNLS, Los Alamos National Laboratory, Los Alamos, NM USA: ecke@lanl.gov
[2]Laboratoire de Physique, École Normale Supérieure de Lyon, Lyon France

Abstract

Stably stratified shear layers are present in many geophysical contexts from oceanic overflows to river estuaries and have been studied in many contexts in both laboratory experiments and numerical simulations. We consider here laboratory experiments on a gravity current where the current itself is turbulent [1] with a Reynolds number of a few thousand (Taylor Reynolds number of about 100) whereas the surrounding fluid is quiescent. The stability of the current is governed by the Richardson number $Ri_0 = g(\delta\rho/\rho)H/U_0^2$ where g is gravity, H is the current thickness, U_0 is the current velocity, and $\Delta\rho << \rho$ is the density difference between the two fluids. Evaluating this system at the exit of our wall-bounded wall jet, we have $0.25 < Ri_0 < 1.0$. The interface between lighter and heavier fluid can be disrupted by local instability, see Fig. 1(a), where turbulent kinetic energy

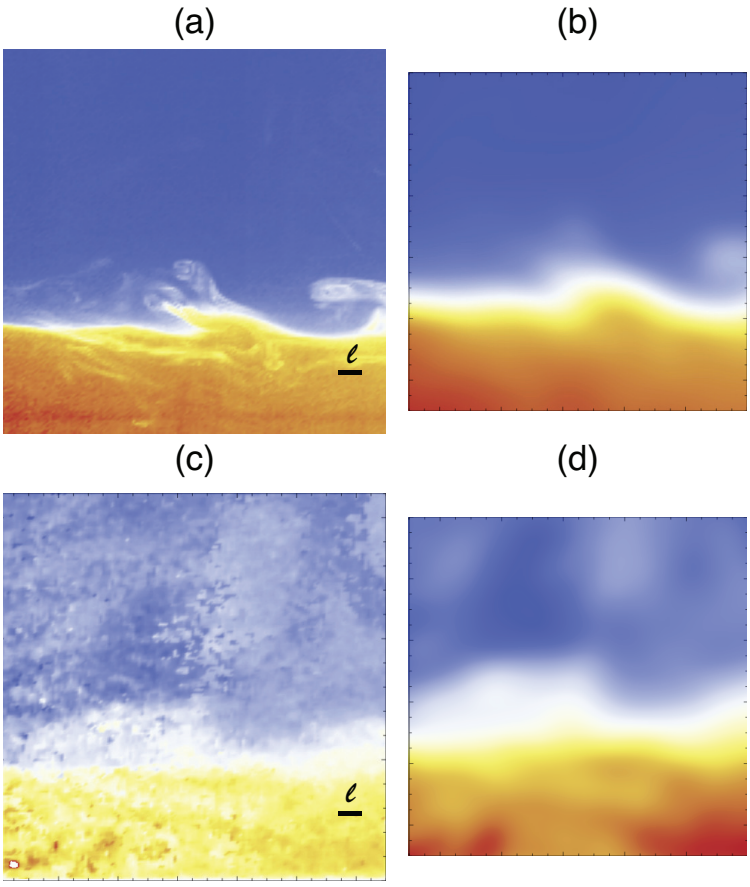

Figure 1: Spatial fields of turbulent gravity current: (a) density ρ, (b) filtered $\overline{\rho}$, (c) downstream velocity u, and (d) filtered $\overline{u}$. The filter length scale ℓ is indicated in (a) and (c). False color imaging where blue is low, red is high and white is intermediate. The filtered fields are smaller by 2ℓ in each direction than the unfiltered fields.

resident in the current or generated by shear at the interface produces overturning and

mixing. Alternately, at the larger range of Ri, the interface may oscillate vertically owing to wave motion while remaining sharp in terms of its local width. This convolution of effects causes problems for the conventional statistical analysis approaches of turbulent flows. Typically, one employs a Reynolds-averaged Navier Stokes (RANS) method, especially useful for experimental data where one may have incomplete information about the flow fields - perhaps measurements at a single point or along a vertical line. A RANS averaging approach, however, convolves the effects of wave motion, large-scale coherent structures and small-scale turbulent transport so a different statistical analysis method is needed.

In cases where the experimental data consist of highly resolved spatial *fields*, it is straight forward to obtain the spatial distribution of turbulent energy flux and of buoyancy flux (as well as many other quantities) using a filtering approach [2, 3] that is utilized in large-eddy-simulations as a computational tool but which can also be used as an analysis method. Indeed, this filter approach has been used for analyzing experimental data in two-dimensional turbulence and direct numerical simulation data in a number of situations [4, 5, 6]; we extend it here to experimental data on stratified shear flows.

The system we consider is one of two miscible fluids undergoing a gravity current flow [1] which consists of a jet of lighter fluid with density ρ_0 exiting a nozzle of height H and width $W >> H$ into a reservoir of heavier fluid with density ρ_1. The flow is constrained from the top by a horizontal smooth boundary which imposes a no-slip boundary condition. The density difference is small compared to the mean density so the Boussinesq equations provide an appropriate description of the flow. We normalize velocity by a characteristic velocity of the current U_0, length by the characteristic height of the current H, pressure by ρU_0^2, and density difference by $\Delta\rho = \rho_1 - \rho_0$. The latter normalization gives a dimensionless density $\theta(\mathbf{x},t) = (\rho_1 - \rho(\mathbf{x},t))/\Delta\rho$ such that $\theta = 1$ for the pure lighter fluid deep inside the current and $\theta = 0$ for pure heavy fluid far outside the current. With the condition of fluid incompressibility, the resulting non-dimensional equations are

$$\begin{aligned}
\partial_t \mathbf{u}(\mathbf{x},t) + \mathbf{u}(\mathbf{x},t)\cdot\nabla\mathbf{u}(\mathbf{x},t) &= -\nabla P + Re^{-1}\nabla^2\mathbf{u}(\mathbf{x},t) + Ri\ \ (1-\theta(\mathbf{x},t))\,\hat{z} \\
\partial_t\theta(\mathbf{x},t) + \mathbf{u}(\mathbf{x},t)\cdot\nabla\theta(\mathbf{x},t) &= Re^{-1}Sc^{-1}\nabla^2\theta(\mathbf{x},t) \\
\nabla\cdot\mathbf{u}(\mathbf{x},t) &= 0
\end{aligned}$$

where the dimensionless control parameters are the Reynolds number $Re_0 = U_0 H/\nu$, the Richardson number $Ri_0 = g(\Delta\rho/\rho)H/U_0^2$, and the Schmidt number $Sc = \nu/D$ with kinematic viscosity ν and mass diffusivity D; bold variables indicate vectors.

Filtering consists of applying a smoothing function to the velocity and density, e.g., $\overline{\mathbf{u}}(\mathbf{x},t) = \int G_\ell(\mathbf{x}-\mathbf{r},t)\,\mathbf{u}(\mathbf{x},t)\,d\mathbf{r}$ (similarly for θ) where $G_\ell(\mathbf{r}) = \ell^{-n}G(r/\ell)$ and $G(r) = \frac{1}{\sqrt{2\pi}}e^{-r^2/2}$ [2, 3, 6]. In Figure 1, we show example raw and filtered images, respectively, of density, Figs. 1(a),(b), and downstream velocity, Figs. 1(c),(d), for a horizontal turbulent gravity current with gradient Richardson number $Ri_0 \sim 1$. For these conditions the interface is relatively stable and the instability is primarily Holmboe-like [7], see Fig. 1(a), rather than the more energetic and overturning Kelvin-Helmholtz instability observed for smaller Ri_0 [1].

Applying filtering to the momentum and density equations results in dynamical equations for the large-scale (low-pass filtered) fields:

$$\begin{aligned}
\partial_t\overline{\mathbf{u}} + \overline{\mathbf{u}\cdot\nabla\mathbf{u}} &= -\nabla\overline{P} + Re^{-1}\nabla^2\overline{\mathbf{u}} + Ri\ \ \left(1-\overline{\theta}\right)\hat{z} \\
\partial_t\overline{\theta} + \overline{\mathbf{u}\cdot\nabla\theta} &= Re^{-1}Sc^{-1}\nabla^2\overline{\theta}
\end{aligned}$$

The linear terms produce averaged quantities of the same form as the unfiltered equation (e.g., the incompressibility condition is the same) but the nonlinear terms produce additional terms that couple among spatial scales (scale transport) and between space points (space transport):

$$\begin{aligned} \partial_t \overline{\mathbf{u}} + \overline{\mathbf{u}} \cdot \nabla \overline{\mathbf{u}} &= -\nabla \overline{P} + Re^{-1} \nabla^2 \overline{\mathbf{u}} + Ri \ \left(1 - \overline{\theta}\right) \hat{z} + \nabla \cdot \tau_\ell \\ \partial_t \overline{\theta} + \overline{\mathbf{u}} \cdot \nabla \overline{\theta} &= Re^{-1} Sc^{-1} \nabla^2 \overline{\theta} + \nabla \cdot \mathbf{b}_\ell \end{aligned}$$

where $\tau_{i,j} = \overline{u_i u_j} - \overline{u_i}\ \overline{u_j}$ and $b_i = \overline{u_i \theta} - \overline{u_i}\ \overline{\theta}$ with subscripts i and j indicating vector (or tensor) components.

One can then obtain the energy budget from the filtered momentum equation and the advection-diffusion transport from the θ equation:

$$\begin{aligned} \partial_t \left|\overline{\mathbf{u}}\right|^2 /2 + \nabla \cdot \mathbf{J}_\ell &= -\pi_\ell + Re^{-1} \left|\nabla \overline{\mathbf{u}}\right|^2 + Ri \ \overline{\mathbf{u}} \cdot \hat{z} \left(1 - \overline{\theta}\right) \\ \partial_t \overline{\theta} + \nabla \cdot \left(\overline{\mathbf{u}} \overline{\theta} - \mathbf{b}_\ell\right) &= Re^{-1} Sc^{-1} \nabla^2 \overline{\theta} \end{aligned}$$

where $J_j\left(\mathbf{x}\right) = \overline{u}_j \left|\overline{\mathbf{u}}\right|^2 /2 + \overline{p u}_j + \overline{u}_i \tau_{i,j} - \nu \partial_j \left|\overline{\mathbf{u}}\right|^2 /2$ represents the mechanisms that act to redistribute energy in space owing to large-scale flow, large-scale pressure, turbulence, and viscous diffusion, respectively. The term $\pi_\ell\left(\mathbf{x}, t\right) = \overline{S}_{i,j} \tau_{i,j}$, where the large-scale strain tensor $\overline{S}_{i,j} = \left(\partial_j \overline{u}_i + \partial_i \overline{u}_j\right)/2$, accounts for energy transferred between spatial scales less than ℓ to/from scales greater than ℓ at any point in the flow at any instant of time. The Galilean invariant property of π_ℓ implies that the energy cascade is independent of the velocity of the observer.

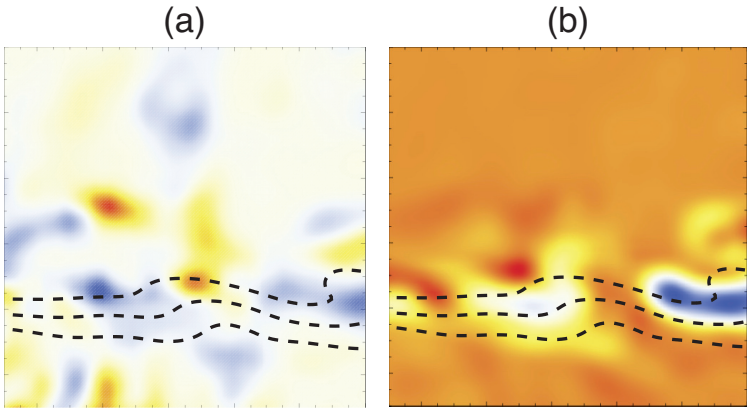

Figure 2: (a) The kinetic energy flux field $\pi_\ell(x, z)$ obtained from the filtering approach. (b) The vertical component of the buoyancy flux field b_ℓ from filtering. The dashed black lines indicate contours of constant density in the filtered density field and roughly brackets the location of the interface.

In this paper, we focus on the behavior of the energy flux π_ℓ and the point-to-point transport of θ. The latter tells us something about the instantaneous transport of density differences by small-scale (less than ℓ) turbulent fluctuations. In Figure 2, we show the resultant scale-to-scale energy flux π_ℓ and the vertical buoyancy flux b_ℓ obtained using the filter approach with a representative value of filter length $\ell = 0.56$ cm which is large compared to the grid spacing 0.056 cm and small compared to the large scale dimensions of the flow $\sim$ 5 cm. This type of analysis allows for a spatial correlation of specific features of instability observed in Fig. 1(a) with energy flux and/or buoyancy flux. A more complete analysis involves the variation of the the filter length ℓ and the resultant dependence of quantities on this spatial scale.

To illustrate some of the important characteristics of the weakly-unstable state at larger $Ri_0 \sim 1$, we consider a series of 166 images spanning about 100 seconds taken at a frame rate of 1.75 Hz. We determine the contour of normalized density $\theta = 0.5$ in the filtered field and use this criterion to divide the flow into a gravity current region and an outer region. In Figure 3, we show $\langle\overline{\theta}\rangle = (1/A)\int_A \overline{\theta} dxdz$ (the brackets indicate the areal average) as a function of time with the area of the gravity current shown in the inset. $\langle\overline{\theta}\rangle$ varies on several time scales: short term frame-to-frame variations, an approximate 10-20 second variation associated with instability structures (see the upper inset of Fig. 2), and an overall variation on the the 100 second time scale. The lower inset shows that the gravity current area increases by about 50% over the 100 seconds, making a RANS averaging problematic. We believe that this long time variation is related to long-wavelength gravity waves at the interface but our experiment cannot determine the properties of these structures directly.

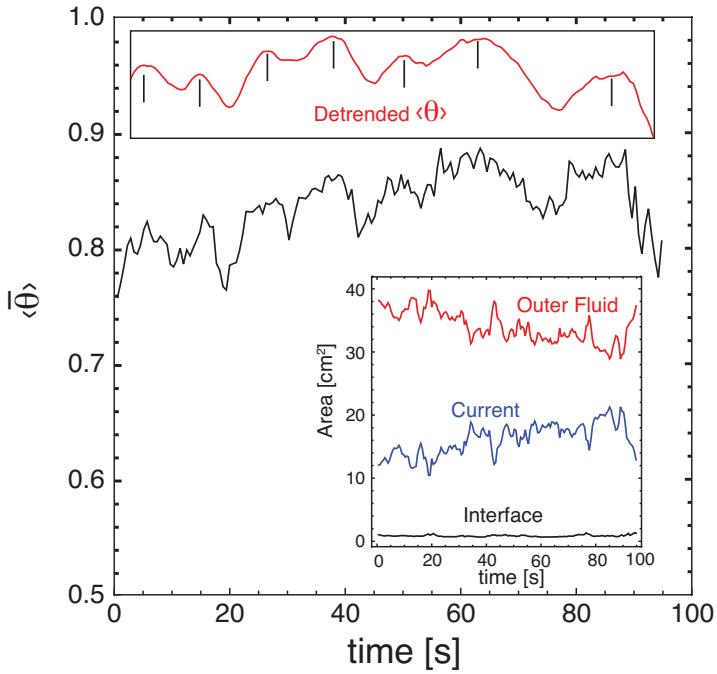

Figure 3: $\langle\overline{\theta}\rangle$ vs time. Lower inset shows the area of the current (blue), the area outside the current (red), and the area of the interface (black) that brackets density contours $0.45 < \overline{\theta} < 0.55$. Upper inset shows a moving average (10 s) and linearly detrended $\langle\overline{\theta}\rangle$ vs time where vertical black lines show local maxima associated with intermediate scale wave motion.

We can also characterize the turbulent properties of the gravity current and its outer field complement. In Fig. 4(a), we show the area-averaged mean energy flux $\langle\pi_\ell\rangle$ for both regions versus time. $\langle\pi_\ell\rangle$ varies considerably with time indicating natural variability in fluctuations generated at the wall and those produced by interfacial instability. The average over the full time series is positive (as are areal averages of a single field) indicating a net forward transfer of energy to small scales with a higher value of the flux for the gravity current $\langle\pi_\ell\rangle = 0.045$ ($\sigma_\pi \approx 9\langle\pi_\ell\rangle$) compared to the outer region $\langle\pi_\ell\rangle = 0.015$ cm^2/s^3 ($\sigma_\pi \approx 15\langle\pi_\ell\rangle$) where turbulent fluctuations arise primarily from the perturbing effects of the current itself. In Fig. 5, we show the probability distribution functions (PDF) for π_ℓ inside and outside of the current. Both show the characteristic positive skewness of forward energy transfer and large forward and backscatter contributions - average forward turbulent transfer results from the small difference of large positive and

negative quantities. We next consider the advective transport of density using the filter approach.

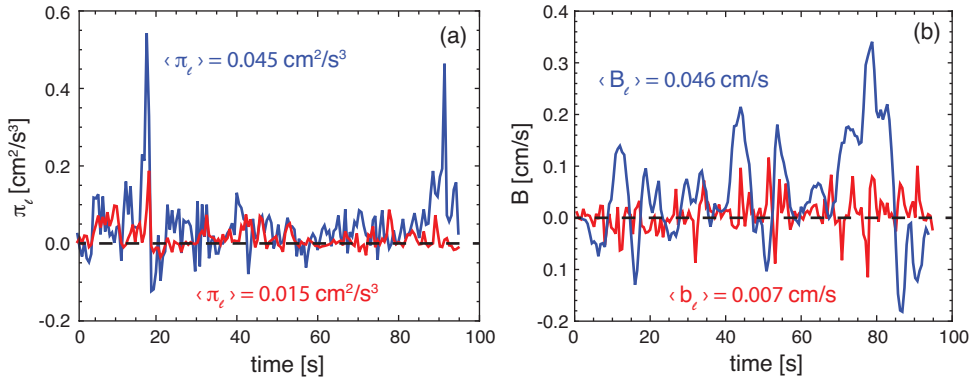

Figure 4: (a) $\langle \pi_\ell \rangle$ vs time. (b) $\langle b_\ell \rangle$ vs time. Blue curves in both indicate averages over the region of the current whereas red curves show values for outside the current. Mean values of the time series are indicated on the plot in the corresponding color.

One of the important quantities in stably stratified shear flows is the entrainment of fluid by the gravity current. We can also analyze this quantity through the filter equations. Ignoring the diffusion term in the equation for θ and integrating over a constant density contour in the filtered θ field [1] yields three terms:

$$\partial_t \int_A \overline{\theta} dA = - \oint_\varsigma \left(\overline{\mathbf{u}}\, \overline{\theta} - \mathbf{b}_\ell \right) \cdot \mathbf{d}\varsigma,$$

where ς is a contour enclosing the area A. This method is very similar to the conditions considered using the RANS approach in [1]. In principle, we can evaluate all of the terms above so that we separate the time dependence of the area-averaged normalized density (see Fig. 3, the transport (stirring) by the mean flow $B_\ell = \overline{u}\overline{\theta}$, and the point-to-point transport of density by small scale turbulent fluctuations b_ℓ. For simplicity, we only consider the vertical transfer component as a demonstration of the power of the approach. In Fig. 4 (b), we show the areal average over a narrow contour band $0.45 < \theta < 0.55$ for B and b. For the case considered here, B is significantly larger, probably indicating that the main vertical transport is by localized coherent structures arising from interfacial instability (e.g., Holmboe instability). In this example, we have not included the dot-product with the contour normal or the contribution of the horizontal component of velocity [1]. A full density transport budget would also include the flux into and out of the current area through the lateral contours ($x = x_0$ and $x = x_0 + L$).

Finally, we show in Fig. 5(b) the PDF of the turbulent vertical flux field $\langle b_\ell \rangle$ for the gravity current region. This PDF has very wide tails and is more symmetric than the energy flux PDFs. More detailed interpretation of the form of the buoyancy flux PDF is outside the scope of the present work and will be discussed elsewhere. Nevertheless, one observes that as with energy transfer there is very large forward and backward fluctuations with very small mean values.

In addition to energy flux and buoyancy flux, one can evaluate some of the other turbulent transport terms that arise in the filtering formalism. This approach may also be quite useful in understanding the spatial structure of turbulent instability, going beyond the RANS approach: the filtering approach was used in this way to elucidate the physical mechanisms of enstrophy and energy transfer in two-dimensional turbulence[4, 5]. The

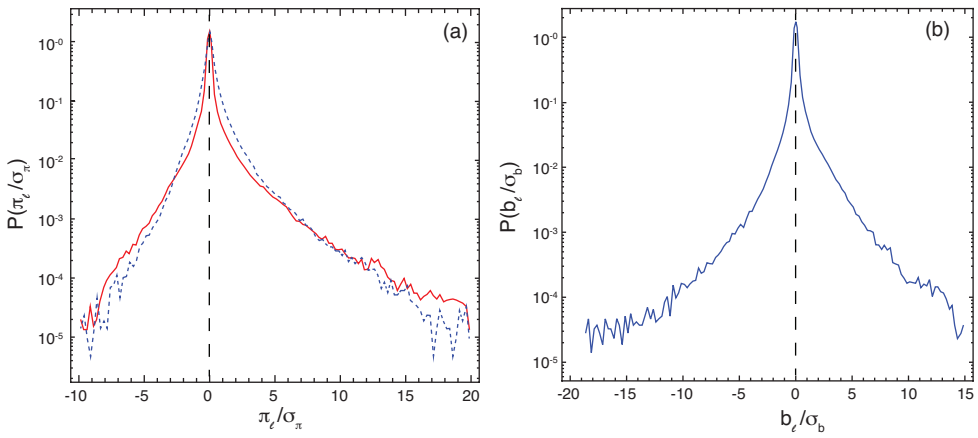

Figure 5: (a) PDF of π_ℓ normalized by σ_π for the gravity current (blue, dashed) and outside the current (red, solid). (b) PDF of buoyancy flux field b_ℓ normalized by σ_b for inside the gravity current.

point of this short paper is to illustrate the types of quantities that one can obtain using the filter approach and how it provides a complementary analysis approach to traditional RANS averaging. To summarize, the filtering approach presents a powerful analysis method when high-resolution data *fields* are available.

This work was carried out under the auspices of the National Nuclear Security Administration of the U.S. Department of Energy at Los Alamos National Laboratory under Contract No. DE-AC52-06NA25396.

References

[1] P. Odier, J. Chen, and R.E. Ecke. Entrainment and mixing in a laboratory model of an oceanic overflow. *J. Fluid Mech* **746**, 498 (2014).

[2] M. Germano. Turbulence - The filtering approach. *J. Fluid Mech.* **238**, 325 (1992).

[3] G. Eyink. Local energy flux and the refined similarity hypothesis. *J. Stat. Phys.* **78**, 335 (1995).

[4] M.K. Rivera, W. Daniel W, S.-Y. Chen SY, and R.E. Ecke. Energy and enstrophy transfer in decaying two-dimensional turbulence. *Phys. Rev. Lett.* **90**, 104502 (2003).

[5] 90 S.-Y. Chen SY, R.E. Ecke, G.L. Eyink, M.K. Rivera, M.P. Wan, and Z. Xiao. Physical mechanism of the two-dimensional enstrophy cascade. *Phys. Rev. Lett.* **96**, 084502 (2006).

[6] M. K. Rivera, H. Aluie, and R.E. Ecke. The direct enstrophy cascade of two-dimensional soap film flows. *Phys. Fluids* **26**, 055105 (2014).

[7] A. Guha and G. A. Lawrence. A wave interaction approach to studying non-modal homogeneous and stratified shear instabilities. *J. Fluid Mech.* **755**, 336 (2014).